Catalysis Today 455 (2025) 115318

Contents lists available at ScienceDirect

Catalysis Today

journal homepage: www.elsevier.com/locate/cattod

Influence of CO_2 presence on propane conversion routes over Cr- and Ga-doped $PtCe/Al_2O_3$ catalysts

D. Ballesteros-Plata [a], I. Barroso-Martín [a], J.A. Cecilia [a], P. Concepción [b], J.M. López Nieto [b], E. Rodríguez-Castellón [a], A. Infantes-Molina [a,*]

[a] Departamento de Química Inorgánica, Cristalografía y Mineralogía, Facultad de Ciencias, Instituto Interuniversitario en Biorrefinerías I3B, Instituto de Materiales y Nanotecnología IMANA, Universidad de Málaga, Campus de Teatinos, Málaga 29071, Spain

[b] Instituto de Tecnología Química, Universitat Politècnica de València-Consejo Superior de Investigaciones Científicas, Avenida de los Naranjos s/n, Valencia 46022, Spain

ARTICLE INFO

Keywords:
Propane
Catalysis
CO_2-ODHP
Noble metal
Ceria
Chromium
Gallium

ABSTRACT

A set of catalysts containing Cr- or Ga-doped Pt-CeO_2 supported on alumina (PCA, Cr-PCA and Ga-PCA) were synthesized by incipient wetness impregnation and tested in propane conversion processes. The catalysts were studied in the propane conversion process with or without CO_2 in the feed. In all cases, an enhancement in stability was found when CO_2 was present in the reaction medium despite the lower catalytic activity. As well, all catalysts presented a higher propylene selectivity in the absence of CO_2, indicating that the direct dehydrogenation of propane is the main reaction route. Moreover, CO_2-assisted propane cracking to ethylene is favoured over propane reforming or direct cracking, given the minimal selectivity to other products like methane. With regards to the catalyst composition, Cr-PCA catalyst was the most active catalyst both in the absence and presence of CO_2, due to the presence of weak acidity and coexistence of Cr^{3+} and Cr^{6+} redox species, as evidenced by XPS analysis. Ga-PCA catalyst was more selective to propylene, indicating that higher acidity of weak-to-medium nature along with formation of low coordinated Ga^{3+} species is beneficial for the CO_2-ODH process. Raman, DTG and XPS analyses after reaction with CO_2 showed that the deactivation of the catalysts was mainly due to carbon deposits of amorphous and graphitic nature on the surface of the catalysts.

1. Introduction

Obtaining basic molecules for the chemical industry through more environmentally friendly and sustainable processes is one of the main issues currently facing the scientific community [1]. Light olefins such as ethylene and propylene are building blocks from which industrial products of enormous value are obtained [2,3], but they are currently co-produced by non-renewable fossil fuel sources through well-consolidated processes like fluidized cracking of light and heavy oil and steam cracking of naphtha [4].

With a compound annual growth rate of 5.6 %, the light olefins market is expected to reach USD 476 million by 2030 [5]. Ethylene stands as one of the most extensively used commodity chemicals worldwide. Its transformation into various everyday items such as plastic packaging, long-lasting goods, personal care products, and other consumer goods underscores its significance. Like ethylene, propylene undergoes conversion into various everyday products such as plastic packaging, durable goods, automotive components and woven fabrics. Polypropylene, the primary derivative of propylene, constitutes approximately 70 % of the global propylene demand [6].

Alkane dehydrogenation processes are the benchmark route to obtain the aforementioned light olefins. However, the thermodynamic limitations associated with direct dehydrogenation have motivated the search for different dehydrogenation reaction pathways overcoming these limitations and, therefore, enhancing alkane conversion and selectivity to the desired products at lower operating costs. In this regard, oxidative dehydrogenation processes using mild to strong oxidants have been established as reference processes to produce light olefins, since the use of oxidants like oxygen favors lower reaction temperatures and it is an exothermic process without thermodynamic limitations [7,8]. However, the selectivity and yield towards the desired products are low (40 % at best) [9,10] due to the formation CO_x species during the deep oxidation of hydrocarbon molecules in the presence of oxygen [8,11–17].

* Corresponding author.
E-mail address: ainfantes@uma.es (A. Infantes-Molina).

https://doi.org/10.1016/j.cattod.2025.115318
Received 15 January 2025; Received in revised form 26 March 2025; Accepted 6 April 2025
Available online 11 April 2025

To overcome the above-mentioned drawbacks, the use of milder oxidants like CO_2 or N_2O has been recently considered [18]. Among the available mild oxidants, the use of CO_2 has attracted special interest, since it implies the valorization of a massive residue that is seriously harming the environment and will surely affect the normal development of future generations. It is not surprising that greenhouse gas (GHG) emissions of anthropological origin are the direct cause of global warming and, therefore, of climate change [2], with CO_2 being directly responsible for around 80 % of global warming [3,19]. In fact, considering that industrial effluents currently account for more than 30 % of CO_2 emissions [20,21], CO_2 valorization processes such as dry reforming of methane (DRM) [22], copolymerization reactions [23], or oxidative dehydrogenation (ODH) of light alkanes [24] are promising alternatives to tackle this global problem and contribute to the circular economy.

Despite the mentioned advantages, the industrial development of this process is still challenging since a deeper knowledge of the reaction mechanisms involved is required to optimize conversions and yields to light olefins, avoiding catalyst deactivation and side reactions.

Whether in the absence or presence of CO_2, alkane dehydrogenation processes are usually accompanied by numerous side reactions that cannot be dismissed. More specifically, in the case of propane dehydrogenation processes, that is the alkane covered in this work, in the presence of CO_2 (CO_2-ODHP, Eq. 1), side reactions like direct Dehydrogenation of Propane (DHP, Eq. 2), Propane Cracking (PC, Eq. 3), CO_2-assisted Propane Cracking (CO_2-PC, Eq. 4), Propane Dry Reforming (PDR, Eq. 5), Water Gas Shift reaction (WGS, Eq.6) and Boudouard reaction (Eq. 7) usually take place simultaneously. Likewise, in direct dehydrogenation processes (DHP, Eq.2) without CO_2, side reactions like propane cracking (Eq. 3) and propane/propylene decomposition and hydrogenolysis of propane could occur [25]. As a result, an overall worsening of the reaction performance and selectivity to propylene could be expected. Moreover, Eq. 6 and 7 that produce CO_x species as byproduct could, in turn, promote reactions in Eqs. 1, 4 and 5. Nonetheless, some of these reactions, especially those in equilibrium, may have a beneficial effect on the overall process. For example, the use of CO_2 provides a continuous supply of oxygen to the reaction, inhibiting coke formation thanks to the reverse Boudouard reaction [10]. Moreover, other valuable products such as ethylene could be obtained.

$$C_3H_8 + CO_2 \rightarrow C_3H_6 + CO + H_2O \quad (1)$$

$$C_3H_8 \rightarrow C_3H_6 + H_2 \quad (2)$$

$$C_3H_8 \rightarrow C_2H_4 + CH_4 \quad (3)$$

$$2C_3H_8 + 2CO_2 \rightarrow 2CO + 2H_2O + 3C_2H_4 \quad (4)$$

$$C_3H_8 + 3CO_2 \rightarrow 6CO + 4H_2 \quad (5)$$

$$CO + H_2O \leftrightarrow CO_2 + H_2 \quad (6)$$

$$2CO \leftrightarrow CO_2 + C \quad (7)$$

The occurrence of the mentioned side reaction has been reported to be strongly related to the catalysts formulation, like its acid-base nature, the use of noble metals or the redox properties of the catalysts [18]. Other factors such as the reaction temperature, the partial pressure of propane or the ratio of inlet gases in the case of the CO_2-assisted process (CO_2/C_3H_8) may also have an impact on the conversion and selectivity.

Regarding the acid-base nature of the catalysts, it has been reported that the presence of strong acidic and basic sites favors the formation of undesired reactions [2], thus, a balance of weak acidic and basic sites is required to avoid side reactions and promote propylene formation [26,27].

Regarding the use of noble metals, platinoids-containing catalysts traditionally used as commercial propane dehydrogenation catalysts given their high propane conversion and propylene selectivity, especially Pt-based catalysts, possess the potential to minimize coke formation during the reaction [28] and/or regenerate active sites [29]. These catalysts are usually supported to stabilize the active phase. Acid solids like Al_2O_3 and tailored mesoporous materials like SBA-15 or MCM-41 have been studied as appropriate supports for noble metals in propane dehydrogenation processes with great stabilization and dispersion of the active phase. Moreover, the use of these tailored materials has also been reported to create new active centres at the metal-support interface [30]. However, the use of noble metals also exhibits notable drawbacks such as the high cost of the noble metal and the catalyst deactivation due to the formation of CO_x species [31]. To overcome them and maximize conversion and selectivity to desired products, the use of non-noble metals with redox and non-redox properties has also been scoped, as well as their combination with noble metals to obtain synergistic effects.

Metal oxide redox catalysts like Cr-, Mo- or V-based catalysts have been thoroughly studied in the DHP reaction [30,32–34], showing high selectivity to propylene but also great deactivation with time in stream due to carbon deposition [35]. Among the redox based catalysts, the chromium-based ones have been widely studied, achieving good catalytic results in the early stages of the reaction [36,37] with Cr^{6+}species being the most active to be reduced to Cr^{3+} or even Cr^{2+} [17,38], but the decrease of $Cr^{6+}/(Cr^{3+}/Cr^{2+})$ ratio with time in stream provokes catalyst deactivation [4,39]. To prevent it, a regeneration process based on steam or diluted air is usually needed for these catalysts, although it eventually leads to irreversible catalyst deactivation. Based on these regeneration processes, the study of CO_2-ODPH on these catalysts has also been scoped. In the presence of CO_2, it has been described that redox catalysts perform the reaction in a single step (Eq. 1) in which the surface oxygen atoms are responsible for propane to propylene conversion and the CO_2 reduction to CO [4,40]. The oxygen mobility on the catalysts' surface is pivotal for the selectivity to propylene, since the lack of oxygen species favours side reactions such as direct dehydrogenation, cracking and dry reforming of propane (Eq. 2, Eq. 4 and Eq. 5, respectively). Both in the presence or absence of CO_2, it can be stated that the presence of Cr^{6+} is crucial to obtain a high activity, since the formation of propylene increases proportionally with the concentration of Cr^{6+}. In fact, Wu et al. [41] studied Chromium oxides catalysts synthesized by gas molecule directing synthesis approach, obtaining highly dispersed Cr^{6+} species on the carrier silicate, attaining 23.6 % propane conversion in the presence of CO_2.

In contrast, non-redox catalysts like those based on Ga have demonstrated great potential to be commercialized as propane dehydrogenation catalysts. In fact, the BP-UOP Cyclar (British Petroleum-Universal Oil Products) process uses Ga supported on ZSM-5 for the direct dehydrogenation of propane and butane to light olefins and aromatics [42]. However, it has also been reported for Ga-based catalysts that in direct dehydrogenation of propane, the propylene selectivity is inversely proportional to the propane conversion, with great influence of both propane partial pressure and acid-base properties of the catalyst on the overall process [43]. Although the nature of the active sites in Ga-based catalysts is still a matter of debate, these catalysts are regarded as excellent activator of C-H bonds rather than C-C bonds [31]. In fact, Michorczyk et al. [44] studied the influence of the modification of acidic and basic properties on the catalytic activity in this process, concluding that the propane dehydrogenation to propylene takes place at Lewis acid sites, which have been reported to be mainly provided by tri-coordinated Ga^{3+} sites [45]. More recently, Oliveira et al. [46] studied Pt and Ga-containing MFI zeolites in the direct dehydrogenation of propane, and stated that the superior stability and catalytic performance of Ga-containing catalysts was attributed to the presence of strong Lewis acid sites as well as to the synergy between Brønsted and Lewis acid sites. Ga-based catalysts have also been studied in CO_2-ODHP process, which is believed to be carried out in two steps: a first step, where the direct dehydrogenation of propane takes place, and another step where the RWGS reaction occurs (Eq. 6) [10], during which the

hydrogen produced in the first step is removed.

Nonetheless, the reported yields using the aforementioned redox and non-redox catalysts are still insufficient and most of them present short life cycles despite the use of CO_2 as a mild oxidant and stabilizer [47]. Therefore, together with the study of different supports, the addition of promoters has been studied. Ceria, thanks to its redox properties, has been used in catalysis due to its ability to store and release oxygen. Moreover, it exhibits the capability to break the C-O bond of the O-C-O molecule, thereby generating a free oxygen atom that can easily interact with the catalyst [48]. Consequently, the incorporation of such metals has the potential to enhance both the catalytic activity and the stability of the catalysts. Moreover, the combined use of ceria and noble metals is considered to have synergistic effects. For instance, Pd has been used to improve stability in $CeZrAlO_x$ based catalyst [49]. The incorporation of Pd enhances the activity of Ce^{3+}-Ce^{4+} sites, improving the conversion without decreasing the selectivity to the desired products. Other studies have shown a strong interaction between Pt and Ce at high temperature, which favoured the reduction of Ce^{4+} to Ce^{3+} [50]. Likewise, the use of alkali and alkaline earth metals have been proposed, with varying degrees of improvement depending on the metal used as active phase [51, 52]. For example, the use of K in Ga-based catalysts has been reported to have negligible influence on the ethane hydrogenation [53].

Considering the wide variety of catalysts used in propane dehydrogenation reaction, in this work the authors have synthesized a set of supported catalysts containing several metals as dopants to either boost conversion or promote the obtention of propylene. Like so, alumina has been chosen as the support to obtain highly dispersed active phases on an acidic support, Pt has been added due to its well-known dehydrogenating capability, Ce for its strong interaction with Pt that may improve conversion and, lastly, Cr and Ga have been incorporated into the catalyst's formulation as redox and non-redox counterparts, respectively. Therefore, the aim of this work is the study of the influence of the metal type and the CO_2 presence on the stability, catalytic activity, selectivity and propane dehydrogenation reaction mechanism.

2. Experimental

2.1. Catalyst Preparation

Water solutions containing the desired amounts of platinum (ammonium tetrachloroplatinate(II), $(NH_4)_2PtCl_4$, 99.9 %, Alfa Aesar) and cerium salts (cerium(III) nitrate hexahydrate, $Ce(NO_3)_3$ 6 H_2O, 99 %, Aldrich) were added to untreated commercial alumina (Al_2O_3 from Alfa Aesar) following the incipient wetness impregnation method. After drying at 60 °C for 24 h and calcination at 600 °C for 6 h (5 °C·min^{-1}), an aqueous solution containing the desired quantity of gallium (puratronic gallium(III) nitrate, $Ga(NO_3)_3$ 6 H_2O, 99.99 %, Alfa Aesar) or chromiun salts (chromium(III) nitrate nonahydrate, $Cr(NO_3)_3$ 9 H_2O, 99 %, Sigma Aldrich) were added following the same procedure. The samples were again dried and calcined under the same previous conditions. The composition of each of the catalysts was: 0.3 wt% of Pt, 1 wt% of CeO_2 and 0.5 wt% of M (with M = Cr or Ga). In all cases, the total metallic load was 1.8 wt% and the molar ratio Pt/Ce/M (1/9/1). The prepared catalysts were denoted as Cr-PCA and Ga-PCA. The sample without Cr or Ga was named PCA.

2.2. Catalytic activity

The catalytic reaction was carried out in fixed-bed quartz reactor with 9 mm of inner diameter and 270 mm of length, the last 100 mm having a diameter of 3 mm to evacuate the reaction gases quickly. The reaction products were analyzed with an on-line Shimadzu GC-2014 gas chromatograph equipped with two columns: i) a Porapak Q 80/100 column to analyze CO_2 and C1-, C2- and C3-hydrocarbons; and ii) a Molecular Sieve 5 A 60/80 column to analyze CO. In the tests, 370 mg of catalyst mixed with 3 cm^3 of silicon carbide were used. In order to choose optimal operating conditions, the reaction was performed without catalyst, observing that neither propane nor CO_2 underwent modifications below 600 °C, however, over this temperature, propane cracking occurred. Thus, the reaction was carried out at 585 °C and atmospheric pressure for five hours. The reaction mixture consisted of 50 mL·min^{-1} of CO_2, C_3H_8 and He, being the CO_2 and C_3H_8 flows 15 and 5 mL·min^{-1}, respectively. The space velocity (GHSV) used was 8108 cm^3·h^{-1}·g$_{cat}^{-1}$, and the ratio of catalyst weight/feed gas flow rate (W/F) was 30.1 g·h·mol$_{propane}^{-1}$. The conversion and selectivity were calculated as follows:

$$\boldsymbol{C_3H_8 Conversion}(\%) = \frac{\boldsymbol{input\ moles\ \ C_3H_8 - output\ moles\ \ C_3H_8}}{\boldsymbol{input\ moles C_3H_8}} \cdot \mathbf{100} \quad (8)$$

$$\boldsymbol{CO_2 Conversion}(\%) = \frac{\boldsymbol{input\ moles\ \ CO_2 - output\ moles\ \ CO_2}}{\boldsymbol{input\ moles CO_2}} \cdot \mathbf{100} \quad (9)$$

$$\boldsymbol{Selectivity}(\%) = \frac{\boldsymbol{n^{o}C product\ moles}}{\boldsymbol{\sum n^{o}C \cdot moles\ of\ component\ produced}} \cdot \mathbf{100} \quad (10)$$

To determine the reaction temperature, tests were carried out without catalyst and at different temperatures with C_3H_8 and CO_2 separately. It was found that below 600 °C propane and CO_2 do not suffer any type of alteration or cracking.

2.3. Characterization techniques

N_2 adsorption-desorption isotherms at −196 °C were used to determinate the BET surface area. For that, it was used an equipment Micromeritics ASAP 2020. Samples were outgassed at 150 °C for 10 h before being analyzed. The High-Resolution Transmission Electron Microscopy (HRTEM) and the Scanning Transmission Electron Microscopy (STEM) images were obtained with a TALOS F200x microscope, and Energy Dispersive X-Ray (EDX) was used to determine the metal particle size distribution in the catalysts. Temperature-programmed desorption of ammonia (NH_3-TPD) was used to analyze the acidity in the fresh catalysts. A Micromeritics AutoChem 2920 equipment was used. For that, prior to analysis, the catalysts (100 mg) were cleaned with He (50 mL·min^{-1}, from 25 to 600 °C, at 10 °C·min^{-1}) in a U-shaped quartz reactor. The system was then allowed to cool to 100 °C, and ammonia flow (10 % NH_3 in He) was passed through for 15 minutes. Then, the samples were cooled until 60 °C, and the physiosorbed ammonia was removed of the samples by flowing He (50 mL·min^{-1}) for 30 minutes. After that, the temperature was increased to 600 °C (10 °C·min^{-1}) with the same He flow to record the ammonia desorption curve for each sample. The surface composition of the sample containing chromium was analyzed by X-ray photoelectron spectra (XPS) with a Physical Electronics PHI 5701 spectrometer with a non-monochromatic Mg-Kα radiation (300 W, 15 kV, 1253.6 eV) and a multi-channel detector. The C 1 *s* signal of adventitious carbon at 284.8 eV was used as reference. Thermogravimetric Analysis (TGA) was used to measure the amount of coke deposited on used catalysts by means of a TA Instruments Mettler Toledo. The analysis was carried out by heating the used catalysts up to 900 °C (10 °C·min^{-1}) in air flow (40 mL·min^{-1}). The percentage of carbon deposited was determined by elemental chemical analysis (CHN) with a Perkin Elmer 240 C equipment. Raman spectra were performed on a Spectrometer-Microscopy Raman Senterra from Bruker to know the nature of the deposited carbon. Samples were measured with the 532 nm excitation line at a power between 2 and 5 mW. The exposure time used was between 10 and 20 seconds, and the number of accumulations was 10. An Olympus 20x long focal length objective was used, and the measurements were made at 25 °C.

3. Results and discussion

3.1. Fresh catalysts characterization

Fig. 1 shows the N_2 adsorption-desorption isotherms at −196 °C and the pore size distribution from the BJH method applied to the desorption branch of the isotherm corresponding to the fresh (Fig. 1) and used (Fig. 8) catalysts. The corresponding isotherms are of type IV (Fig. 1a) according to IUPAC [54], characteristic of mesoporous materials.

The hysteresis loop is of H2(b) type, although considering its closure without plateau it could be said to be H4. In addition, the shape of the hysteresis loop also indicates pore blocking or percolation with large distribution of narrow neck widths [53]. The presence of micropores in the samples is observed by the steep initial slope at low relative pressures, although the proportion of mesopores is much higher, as can also be seen in the pore size distribution graphs (Fig. 1b), with an average pore diameter of 50 Å as collected in Table 1.

As for the calculated BET values, the results are in good agreement with those reported for Pt-Ce-Al_2O_3 systems [55]. When Pt and Ce are incorporated into alumina, the specific surface area decreases slightly, as after the incorporation of Cr and Ga into PCA, where a negligible decrease is observed given the low metallic loading and the nanometric size of the metallic particles, as observed in the TEM images in Fig. 2.

High-resolution transmission electron microscopy analysis coupled to EDX analysis (Fig. 2) revealed that the metallic particles are homogenously dispersed on the alumina support. In the case of the bare PCA catalyst, a more uniform and smaller particle size was found for both Pt and Ce according to the particle size distribution of each element. It is observed that, although some sintering may have taken place given the increase in Pt particle size (which is expected due to the high reaction temperature), the catalyst remained quite stable after reaction. When Cr or Ga was added to the catalyst formulation, an increase in the Pt, Ce and Cr or Ga particle size, as well as a broader particle size distribution, is clearly noticeable. In the case of Cr, a decrease in the particle size is evident after reaction, which could be related to the Cr_2O_3 to CrO_3 transformation due to oxidation during the reaction.

On the contrary, the Ga particle size remained stable. Nonetheless, all metallic particles were below 6 nm in all cases, as previously reported for Pt/CeO_2-Al_2O_3 systems [56].

The total weight percentage of metals in the prepared catalysts obtained from EDX spectra is collected in Table 2 and are in accordance with the nominal values except for Pt in PCA, with a much higher value. Although STEM-EDX is a local analysis, it could be suggested that this fact could be related to the smaller particle size found in this sample (1.59 nm *vs* 4.1 nm and 5.2 nm for Cr-PCA and Ga-PCA, respectively) and to the higher dispersion of Pt in this catalyst.

Table 1
Summary of the textural properties of the catalysts.

Sample	S_{BET} ($m^2 \cdot g^{-1}$)	V_p ($cm^3 \cdot g^{-1}$)	d_p (Å)
Cr-PCA	135	0.21	50.3
Ga-PCA	134	0.23	49.9
PCA	140	0.24	49.2
Al_2O_3	150	0.23	48.1

The acidic properties of the prepared samples were evaluated from ammonia thermo-programmed desorption tests (NH_3-TPD) and the registered profiles are displayed in Fig. 3. All desorption profiles presented a broad band between 60 and 450 °C. Typically, the ammonia thermo-programmed desorption profiles can be divided into three regions: Zone I in the range of 60–200 °C, which indicates weak acidity; Zone II between 200 and 300 °C, indicating active sites with medium acidity; and Zone III, from 300 to 600 °C that implies strong acidity. The desorption profiles for the prepared samples were integrated considering the mentioned zones, and the quantification of each one is collected in Table 3 as the number of acid centers per gram of catalyst ($\mu mol_{NH3} \cdot g^{-1}$) and as normalized acidity per surface area ($\mu mol_{NH3} \cdot m^{-2}$).

All samples showed a desorption profile similar to that reported for Pt-Ce-Al_2O_3 systems [55,57], mainly due to Al_2O_3, whose acidity is well-studied and related to Lewis acid sites [58]. As already reported, the introduction of Pt and Ce enhances weak and medium acidity and decreases the strong acidity in alumina-based samples [59]. Likewise, some differences are observed when Cr and Ga are added to the catalyst formulation. In Ga-PCA sample, a loss in the weak and strong acid sites is noticeable, while the medium ones remained unaltered compared to the PCA sample, which is expected given the medium strength acidity of Ga_2O_3 [60]. It is also been reported that the medium strength acidity is associated with Ga-O-Al Lewis acid sites and low coordination Ga sites [46,61]. Lastly, the incorporation of Cr provoked a decrease in the acidity, which could be associated with the loss of surface hydroxyl groups of Al_2O_3 due to the Cr anchoring in these species as inferred by XPS results in Fig. 4(e) showing a higher contribution of Cr^{6+} species [62]. Moreover, this finding is in good agreement with the data in Table 3, indicating that the Cr-PCA sample is the one with the highest contribution of weak nature acid sites, which has been reported to be related to the surface Cr^{6+} species, providing additional weak acid sites [63].

XPS measurements were performed to study the chemical environment and the chemical states of the species present on the catalysts' surface. Although the Pt 3*d* signal was registered instead of Pt 4*f* one, since Al 2*p* signal overlaps with the weak Pt 4*f* signal, the obtained

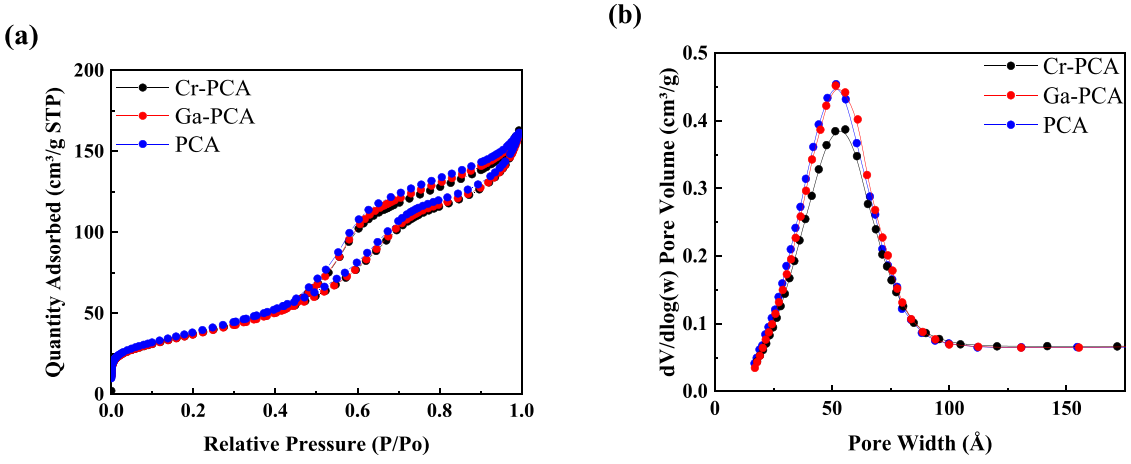

Fig. 1. (a) Nitrogen adsorption-desorption isotherms at −196 °C and (b) pore size distribution of fresh catalysts.

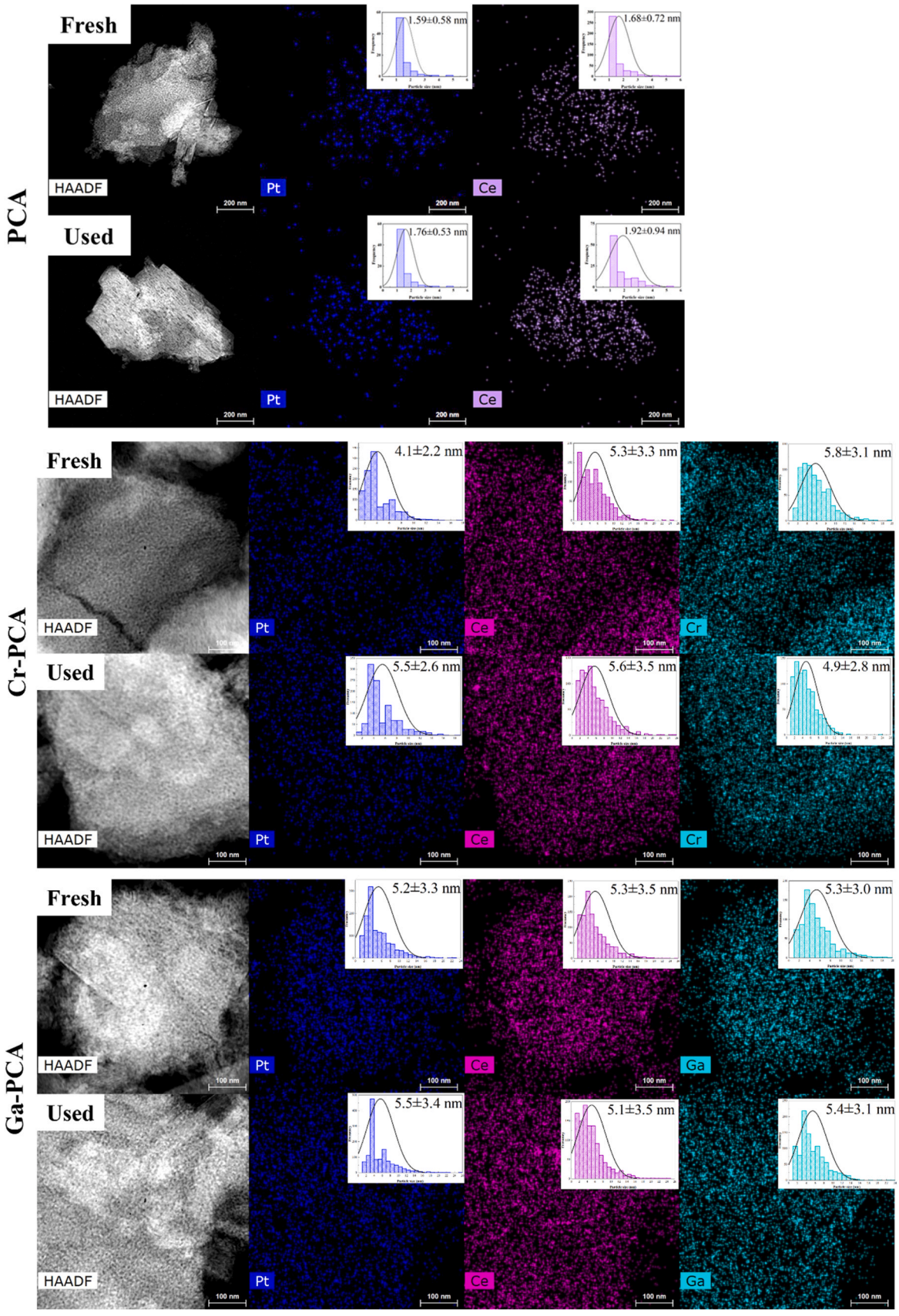

Fig. 2. STEM-EDX micrographs of fresh and used catalysts and particle size distribution in the inset imagen of each element.

Table 2
Pt, Ce and Cr or Ga metal weight percentage of fresh catalysts from EDX analyses. Values in brackets stand for nominal wt% ones.

Metal	PCA	Cr-PCA	Ga-PCA
Pt (0.3)	2.5	0.2	0.3
Ce (1.0)	1.05	0.9	0.8
M* (0.5)	-	0.4	0.4

M* : Cr, Ga.

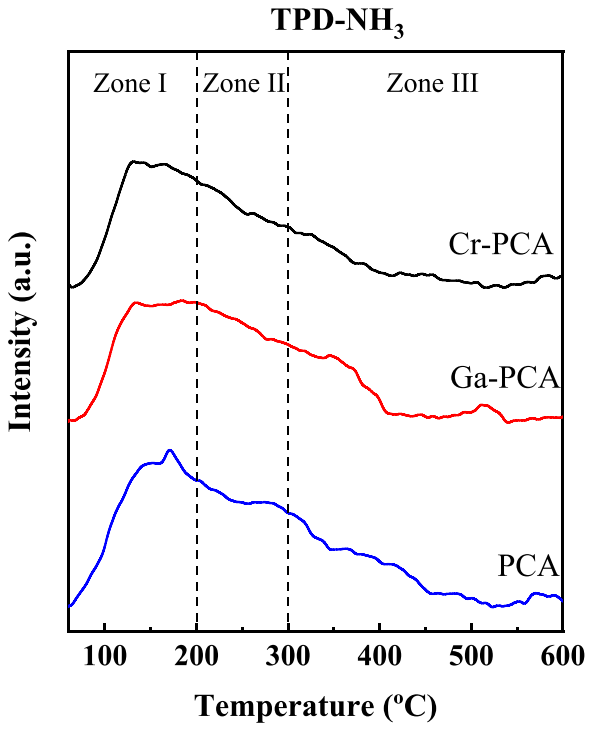

Fig. 3. Ammonia thermo-programmed desorption curves for fresh catalysts.

Table 3
Quantity of desorbed ammonia during NH_3-TPD for fresh catalysts.

Sample	Acidity ($\mu mol_{NH3} \cdot g^{-1}$)[a]				Acidity* ($\mu mol_{NH3} \cdot m^{-2}$)[b]
	Zone I	Zone II	Zone III	Total	
Cr-PCA	139	92	57	288	2.13
Ga-PCA	149	127	78	354	2.64
PCA	170	131	113	414	2.96

[a] Zone I: from 60 to 200 ºC, weak acidity; Zone II: from 200 to 300 ºC, medium acidity; Zone III: from 300 to 600 ºC, strong acidity.
[b] Acidity ($\mu mol_{NH3} \cdot m^{-2}$) calculated from acidity ($\mu mol_{NH3} \cdot g^{-1}$) and superficial area BET ($m^2 \cdot g^{-1}$).

signal was too noisy given the low Pt loading (0.3 wt%) and data is not shown. Al 2*p* in Fig. 4(a) showed a broad peak at 74.1 eV, related to Al^{3+} species from Al_2O_3 [64], and with no significant changes after the addition of Cr or Ga. The O 1 *s* signal in Fig. 4(b) was decomposed in three contributions for all catalysts: the first one at lowest binding energy, 530.1 eV, was attributed to lattice oxygen in metal oxides (M-O bonds with Ce, Pt and Cr or Ga); a main one at 531.1 eV, associated with Al_2O_3; and that at 532.6 eV, related to hydroxyl Al-O-H surface groups and/or oxygen vacancies [65,66]. It is observed in Table 4 that the Ga-PCA catalyst presented greater contribution to oxygen vacancies than Cr-PCA, as already inferred by NH_3-TPD results. Likewise, the bare PCA catalyst was the one with the greatest contribution related to lattice oxygen in metal oxides, which was also slightly shifted to lower binding energy, as previously reported for CeO_2-Al_2O_3 systems [67], indicating that in this sample, CeO_2 is more superficially exposed, which could also explain the higher wt% of Ce found in the EDX analysis for the PCA sample.

Despite the low Ce loading in all samples (1 wt%), Ce 3*d* signals were registered and are displayed in Fig. 4(c), although not decomposed given the low signal-to-noise ratio. Nevertheless, the presence of Ce^{3+} species can be evidenced rather than Ce^{4+} ones, according to the spin-orbits doublets υ_0, u_0, υ', u' at 880.9, 899.2, 885.2 and 903.4 eV, respectively [68]. The coexistence of Ce^{3+} and Ce^{4+} species has already been studied by Damyanova et al. [67], who related it to the broadening in Ce 3*d* signals for Ce-Pt-Al_2O_3 systems with 0.5–1 wt% Ce. Moreover, the prevalence of Ce^{3+} species in these catalysts is associated with a higher amount of non-stoichiometric oxygen [69]. This suggests, as evidenced by the O 1 *s* signals and the NH_3-TPD results, the existence of oxygen vacancies within the material, which are available for the oxidation of propane molecules. These vacancies have been reported to directly attack C-H bond in propane, whose activation energy is reduced on these defective sites, thus its activation by localized electrons is eased [70]. Fig. 4(d) displays the Ga 2*p* core level spectra for the Ga-PCA catalysts, which showed a main signal at 1117.8 eV, attributable to Ga^{3+} species of Ga_2O_3 in Pt-Ga_2O_3/Al_2O_3 systems [71]. Lastly, the Cr 2*p* core level spectrum in Fig. 4(e) was decomposed into 5 contributions considering its overlapping with the O 1 *s* second plasmon satellite at 581.5 eV [72] and both $2p_{3/2}$ and $2p_{1/2}$ spin-orbit doublets (continuous and dashed lines, respectively). Thus, both Cr^{3+} and Cr^{6+} presence was evidenced, with Cr $2p_{3/2}$ bands at 574.8 and 577.4 eV, respectively. The separation of 2.6 eV between bands has been already reported for several chromium-containing compounds [73]. Although higher oxidation states are expected to be found at higher binding energy values, given the low binding energy of the Cr^{3+} peak, the presence of Cr^{4+} cannot be discarded, according to the photo-emission at 575.2 eV reported value by Halada and Clayton [74].

3.2. Study of catalytic activity

First of all, the catalytic perforance of the catalysts for propane dehydrogenation, in the absence of CO_2, was studied. The variation of propane conversion and selectivity to the desired products (i.e., propylene and ethylene) with time on stream are plotted in Fig. 5. From the reaction profile in Fig. 5(a), it is observed that the redox catalyst Cr-PCA suffered severe deactivation as the reaction progressed, decreasing the propane conversion from 24 % to 16 %, probably due to the hindered access to the active sites by carbon deposition, as will be discussed further in the CNH analysis which revealed an increase in % C after the reaction (see Table 7). In addition, the decrease in activity could be associated with the decrease in oxygen mobility due to the anchoring of hydroxyl groups to the Cr^{6+} species formed by the oxidation of Cr^{3+} with time on the stream [62]. Conversely, the non-redox Ga-PCA catalyst remained more stable over the test time, although obtaining lower propane conversions (12 %) than the redox one, which has been associated with the lower C-H activation capability of the Ga_2O_3/Al_2O_3 systems [75]. In the case of the bare PCA, it presented the lowest propane conversion with deactivation over time on stream. This could be related to the higher presence of oxygen vacancies in the quaternary catalysts together with a mainly weak acidity nature, as stated by the XPS and NH_3-TPD results, respectively.

Regarding the selectivity to propylene after 5 hours on stream (Table 5), during the transformation of propane in the absence of CO_2, it can be observed that both Ga-PCA and Cr-PCA (attaining 58 % and 54 %, respectively) show a higher selectivity than that observed for the PCA catalyst (with only a selectivity to propylene of 37 %). These results confirmed that the use of Cr and Ga as promoter has a beneficial effect on propylene production through direct propane dehydrogenation (Eq. 2). Although at early reaction times Cr-PCA resulted more selective towards propylene as displayed in Fig. 5(b), the loss of activity also induces a loss in propylene selectivity, and competitive side reactions such

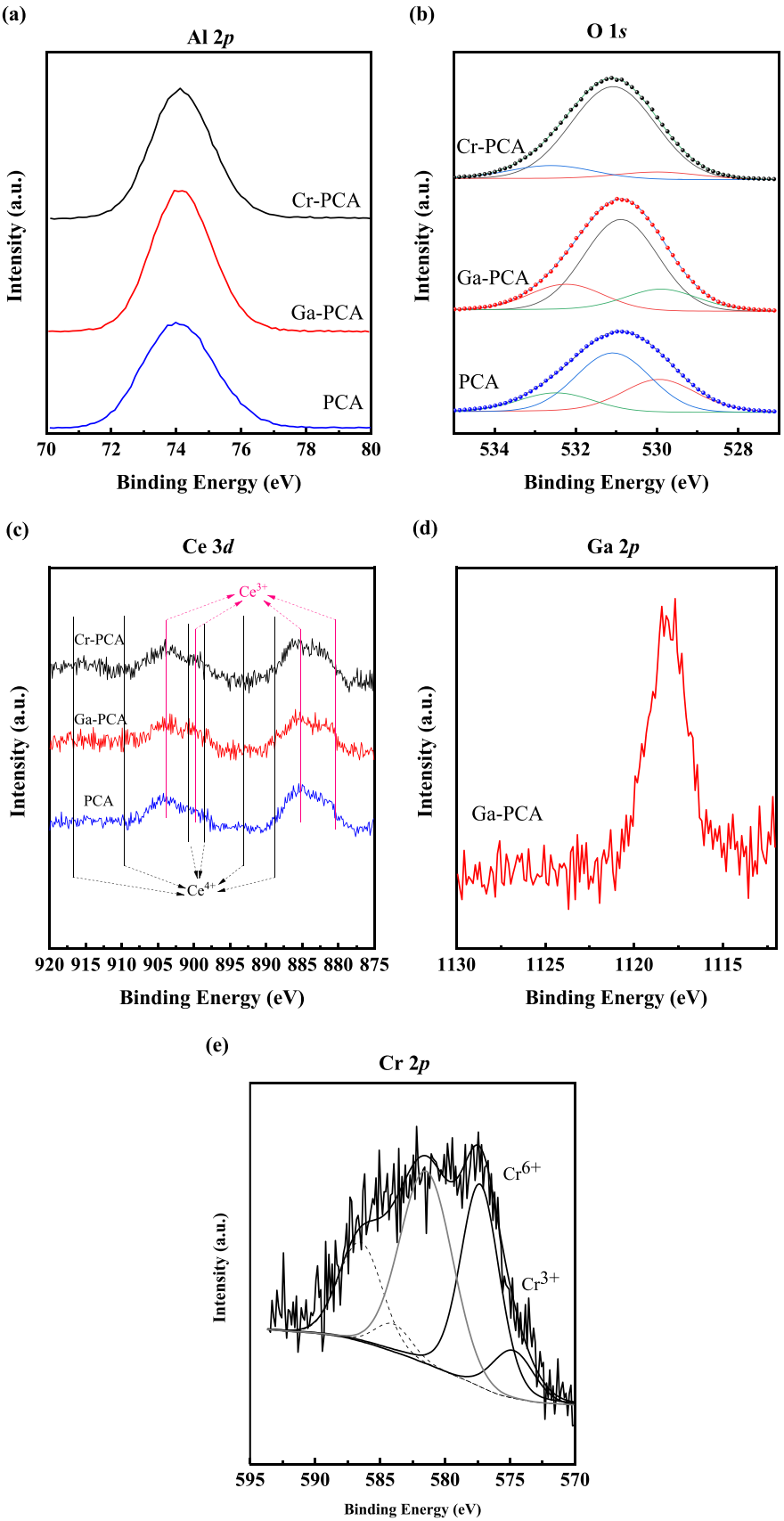

Fig. 4. (a) Al 2*p*, (b) O 1 *s*, (c) Ce 3*d*, (d) Ga 2*p* and (e) Cr 2*p* core level spectra for fresh catalysts.

Table 4
Binding energies for oxygen species (in eV) in the prepared samples. Values in brackets represent percentage of each contribution.

Catalyst	O 1 *s* contributions		
	M-O	Al_2O_3	-OH, Oxygen vacancies
Cr-PCA	530.1 (20)	531.1 (63)	532.5 (17)
Ga-PCA	529.9 (17)	530.9 (65)	532.2 (18)
PCA	529.7 (31)	531.1 (52)	532.5 (17)

Table 5
Products distribution during the propane transformation, after five hours on stream, in the absence and in the presence of CO_2.

Sample	In the absence of CO_2				In the presence of CO_2			
	C_3H_6	C_2H_6	C_2H_4	CH_4	C_3H_6	C_2H_6	C_2H_4	CH_4
Cr-PCA	54.2	3.9	35.0	6.9	24.1	2.9	49.0	7.6
Ga-PCA	58.3	0.0	34.8	6.9	25.1	0.0	62.3	3.0
PCA	36.8	0.0	47.4	8.5	22.2	0.7	61.9	0.6

The rest of the percentage up to 100 % is CO.

as propane cracking (Eq. 3) are favoured, giving rise to ethylene as can be observed in Fig. 5(c).

Interestingly, the Ga-PCA catalyst showed the opposite trend, with increasing propylene formation with time on stream. This fact could be related to the higher weak-to-medium acidity of this catalyst reported by NH_3-TPD results, together with the higher presence of oxygen vacancies evidenced by XPS and the formation of Ga^{3+} and Ga_xO_y species that favour propylene production [75].

For the propane transformation in the presence of CO_2 (Fig. 6), an increase in catalyst stability was observed for all catalysts. This fact highlights that, as previously reported [41], CO_2 has a catalyst reactivation role in propane conversion processes such as CO_2-ODH. However, a decrease in activity was observed in the Cr- and Ga-containing catalysts, as expected [76]. In the Cr-PCA catalyst, the final propane conversion, in the presence of CO_2, was 14 % vs. 16 % in the absence of CO_2. In the case of Cr-based catalysts, Shishido et al. [77] suggested that CO_2 had a promoting effect on the catalytic activity due to the oxidative dehydrogenation of propane at the regenerated Cr^{6+} sites after the Cr^{3+} oxidation to Cr^{6+}. In fact, the predominant presence of Cr^{6+} species was evidenced by XPS analysis of the catalysts. Interestingly, with CO_2, both the Ga-PCA an PCA catalysts presented stable and similar catalytic behaviour. In the case of Ga-PCA, an average propane conversion of 9 % is observed, lower than that obtained in the absence of CO_2 (11 %). On the other hand, PCA even surpassed the Ga-PCA catalyst as the reaction proceeded, reaching 10 % propane conversion (vs. 7 % without CO_2).

Regarding the CO_2 conversion (Fig. 6(b)), it was lower than the propane conversion (Fig. 6(a)) in all cases despite the CO_2-ODH reaction's stoichiometry, which indicates that side reactions that generate CO_2 as a byproduct are also taking place, such as Water Gas Shift (Eq. 6) and Boudouard (Eq. 7) reactions. Cr-PCA showed the highest CO_2 conversion of ca. 7 %, whereas that of PCA was less than 5 %. For the Ga-PCA catalyst, the CO_2 conversion was minimal, less than 1.5 %. This fact is supported by the CNH results in Table 7, that indicated that the % C is increased after the reaction due to coke deposits that may come from the Boudouard reaction, suggesting that Cr and Ga could favour the aforementioned side reactions rather than CO_2-ODH.

Figs. 6(c) and 6(d) display the selectivity to propylene and ethylene, respectively, achieved during propane conversion in the presence of CO_2. The catalyst with the highest propylene selectivity was Cr-PCA, with a small decrease (from 29 % to 24 %) with time on stream. On the other hand, Ga-PCA showed a more stable propylene selectivity of *ca.* 25 %, which could be explained considering that despite the previously mentioned lower C-H activation capability of Ga_2O_3/Al_2O_3 systems, the presence of medium strength acid sites thanks to low coordinated Ga and Ga-O-Al network facilitates propane activation on the Ga-PCA catalyst [61]. On the other hand, PCA also had a stable behavior although the propylene production was slightly lower, closed to 22 %. It is clearly noticeable that the presence of CO_2 worsened the propylene selectivity, decreasing from 54.2 % to 24.1 % in the most active catalyst, Cr-PCA. Conversely, the selectivity towards ethylene is greatly improved according to the results presented in Fig. 6(d) and Table 5. The minimum selectivity towards methane suggests that the ethylene production reaction is taking place via CO_2-assisted propane cracking to form CO and H_2O as byproducts (Eq. 4) rather than via direct propane cracking to ethylene and methane (Eq. 3).

With the aim to evaluate the possible CO_2-ODH reaction pathways and the involved side reactions, the CO/C_3H_6 ratio and the selectivity towards the obtained products were studied. Ratios close to 1 indicate that CO_2-ODH is the main reaction pathway towards propylene, according to Eq. 1, while ratios over 1 indicate that side reactions such as dry propane reforming (Eq. 5) are also taking place [4,40]; and ratios under 1 suggest direct dehydrogenation of propane (Eq. 2) that, as observed in the experiments of this work, eventually leads to catalyst deactivation (see Fig. 5(a)). Fig. 6(e) shows how the incorporation of Cr and Ga into the PCA structure gives rise to more stable CO/C_3H_6 ratios, closer to unity, while bare PCA showed high CO/C_3H_6 ratios around 4 that diminished to 2 as the reaction evolved. Considering the stable selectivity to propylene on this catalyst, around 22 %, the diminishing in the ratio is due to the CO consumption. Thus, side reactions like direct dehydrogenation, WGS and Boudouard reactions are favored with time on stream, which, together with CNH results in Table 7, supports the low CO_2 conversions obtained with this catalyst. More concretely, although the Cr-PCA catalysts present a more stable trend with CO/C_3H_6 ratios close to 1.6, a slight increase is evident as the reaction progresses, achieving CO/C_3H_6 ratios equal to 2 after five hours. Conversely, on the Ga-PCA catalyst, the initial CO/C_3H_6 ratio was close to 2, but a progressive decay was observed after 1.5 hours, reaching a final ratio of 1.1, which indicates that the CO_2-ODH reaction is more favored with the Ga-based catalyst. In fact, according to the Table 5 data, Ga-PCA presented the highest selectivity towards propylene.

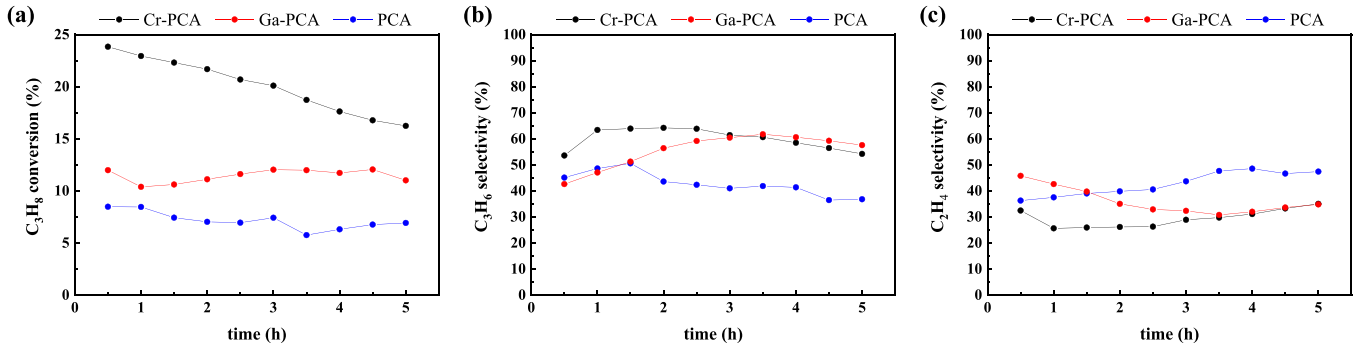

Fig. 5. (a) Evolution of propane conversion, (b) selectivity to propylene and (c) selectivity to ethylene during propane transformation in the absence of CO_2.

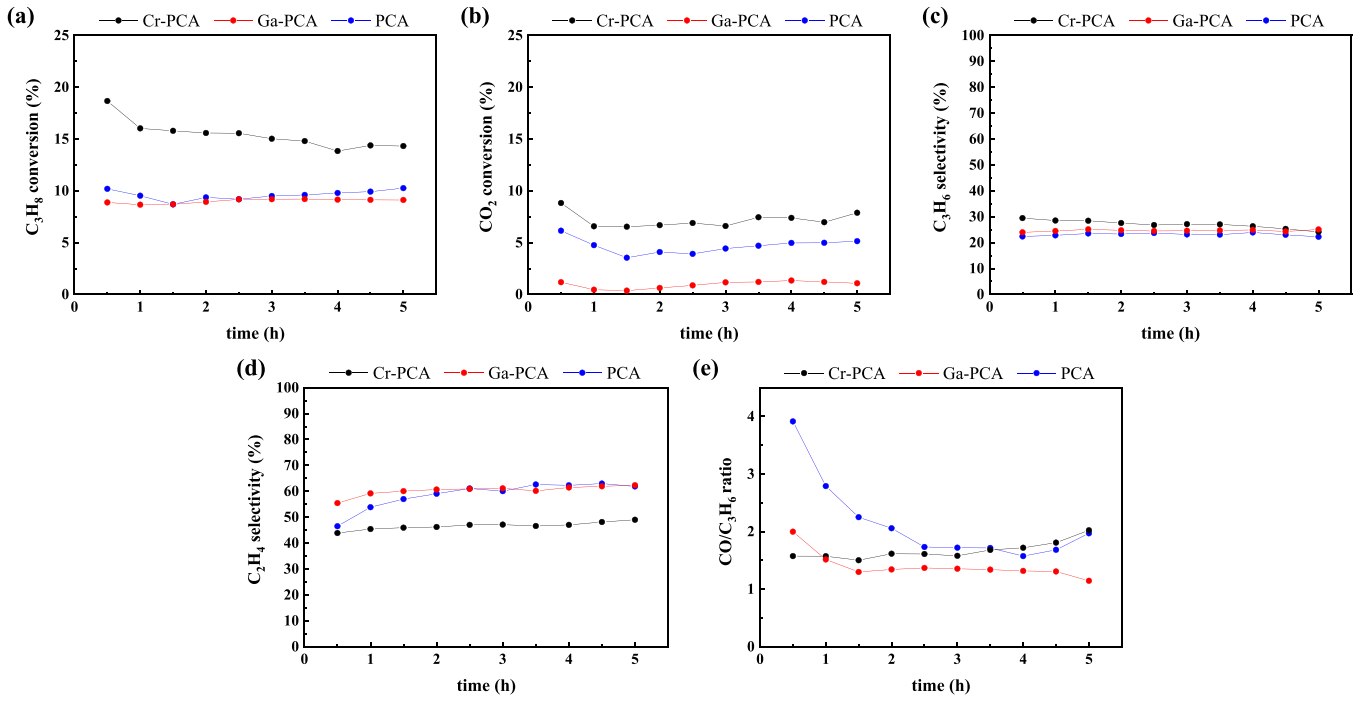

Fig. 6. Evolution of (a) propane and (b) CO_2 conversion, selectivity to (c) propylene and (d) ethylene and (e) CO/C_3H_6 ratio during propane transformation in the presence of CO_2.

3.3. Used catalysts characterization

The catalysts were also studied after the reaction in the presence of CO_2 to assess any changes in the catalysts. Regarding their textural properties (Table 6, Fig. 7), a decreased in the specific surface area of the catalysts is evident after the reaction if data in Tables 1 and 6 are compared, probably due to the pore blocking by carbonaceous deposits. Interestingly, this decrease is less pronounced in the catalysts containing Cr or Ga, which support the catalytic findings mentioned above, i.e., the presence of CO_2 together with the addition of these elements prevents the catalysts' deactivation. This, in fact, will also be suggested by the DTG and CNH results of the used catalysts hereafter. Lastly, regarding the pore size distribution in Fig. 7(b) and Table 6, a slight increase in the average pore width was observed in all cases after the reaction, which could be related to the interparticle voids.

The carbon deposition after five hours on stream determined by CNH elemental analysis (Table 7) reflects the behavior seen in the catalytic tests, being the most active but also the most deactivating, Cr-PCA, the one with the highest % C after the reaction. When CO_2 is present in the reaction medium, an increase in carbon deposition is observed for the Cr-PCA and Ga-PCA catalysts, which could be explained considering that the CO produced during CO_2-ODH (Eq. 1) and CO_2-assisted propane cracking (Eq.4) could be consumed through the Boudouard reaction (Eq. 6), thus increasing C deposits. This fact is also supported by the data found for the PCA catalyst, in which a lower % C is found after the reaction in the presence of CO_2. From the propane and CO_2 conversion profiles (Figs. 6(a) and 6(b)), it is observed that the PCA catalyst was the one with the smallest difference between these conversions, indicating that, on this catalyst, the CO_2-producing side reactions are hindered. Moreover, from the CO/C_3H_6 ratio profile in Fig. 6(e), it is observed that, with respect to PCA, this ratio was greatly diminished during the reaction, confirming that the CO_2-ODH reaction was favored over time on stream.

Raman spectra were recorded to study the chemical structures present after the reaction and the registered signals are collected in Fig. 8 (a). Two main bands are present in all the used catalysts at *ca.* 1597 and 1346 cm^{-1}, which are associated with the G (graphitic) and D (disorder) bands, respectively [78–80]. The presence of the G band is related to the Raman active $E_{2\,g}$ in-plane vibration mode in oriented, large graphite crystals, whereas the D band is associated with $A_{1\,g}$ vibrational mode of amorphous carbon [81]. The intensity of the signals is in accordance with the CNH results, with the catalyst with the highest intensity being Cr-PCA. Conversely, the PCA catalysts showed weak signals and low %C after the reaction, which supports the catalytic test results.

Two other signals are also noticed in quaternary catalysts, at *ca.* 831 and 611 cm^{-1}. The first one is clearer in the Cr-PCA catalyst and could be related to CrO_3 species in its monoclinic phase [78]. The former is due to carbonate species [82] and the last one can be attributed to the existence of a defect-induced mode due to intrinsic oxygen vacancies in CeO_2 lattice [83,84]. This band is more noticeable in Ga-PCA catalyst, indicating that Ga could favour the formation of these oxygen vacancies, as already suggested by XPS and NH_3-TPD results. Likewise, the presence of Cr_2O_3 contribution at 608 cm^{-1} [76] in the Cr-PCA catalyst cannot be discarded, given the slight shift towards lower values of the peak together with its low intensity and broadness and considering that the Cr^{3+} presence was confirmed by XPS in Fig. 4(b).

To distinguish the type of carbonaceous species present in the used samples, differential thermogravimetric (DTG) analysis was carried out. The presence of graphitic and amorphous carbon is confirmed by DTG analysis, as evidenced by the Raman spectra. In Fig. 8(b), an intense weight loss rate peak is observed for the three samples, associated with carbon oxidation processes. Its location at 400 °C is related to the presence of amorphous carbon [85]. Moreover, in the inset of Fig. 8(b), a broader and less intense, peak is noticeable between 600 and 850 °C, associated with graphitic carbon [86]. A shift towards higher

Table 6
Textural properties of the prepared catalysts after reaction in the presence of CO_2.

Sample	S_{BET} ($m^2\ g^{-1}$)	V_p ($cm^3\ g^{-1}$)	d_p (Å)
Cr-PCA-u	118	0.18	52.0
Ga-PCA-u	120	0.19	53.4
PCA-u	104	0.20	53.8

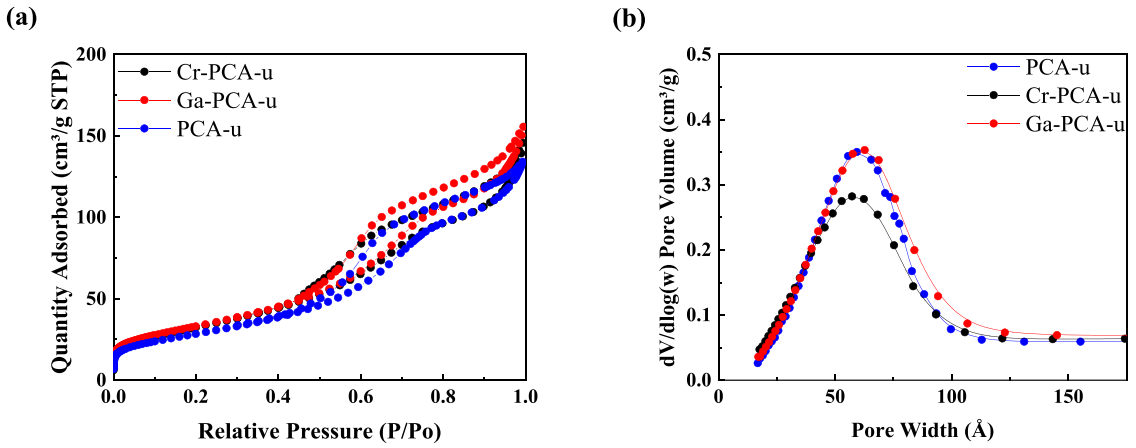

Fig. 7. (a) Nitrogen adsorption-desorption isotherms at −196 ºC and (b) pore size distribution of prepared catalysts after reaction in the presence of CO_2.

Table 7
Carbon (%) deposited in the used catalysts determined by CNH elemental analysis.

Reaction	Cr-PCA-u	Ga-PCA-u	PCA-u
In the absence of CO_2	1.58	0.85	1.06
In the presence of CO_2	3.54	1.19	0.62

temperatures is observed when Ga and Cr are added to the PCA catalyst, suggesting that the loss of M-OH groups is also occurring in these catalysts [87]. The Cr-PCA catalyst showed the most intense signal, which also supports the higher %C found in the CNH analysis of the used samples and the higher deactivation of this catalyst. Lastly, carbonaceous species were studied by XPS analysis of C 1 *s* core level spectra (see Fig. 8(c)). All registered signals could be decomposed into three contributions: a main one at 284.8 eV, associated with adventitious carbon; a second one at *ca.* 286 eV, related to C-OH groups; and the one at the highest BE, ~289 eV, attributed to carbonate species [85,88]. The latter two are more present in the bare PCA catalyst, which could explain the shift to a lower temperature observed in the weight loss rate peak in DTG profile in Fig. 8(b). The Ce 3*d*, Ga 2*p* and Cr 2*p* core level spectra were also recorded for spent catalysts, which did not show significant changes after the reaction in the presence of CO_2. Finally, STEM-EDX analyses (Fig. 2) evidenced a minimal change in particle size after the reaction that catalyst deactivation is not related to particle sintering but to coke deposition and, on the other hand, as evidenced by catalytic results, Cr and Ga enhance the stability of the catalysts.

4. Conclusions

Alumina supported catalysts containing 0.3 wt% Pt, 1 wt% Ce and 0.5 wt% Cr or Ga prepared by incipient wetness impregnation, obtaining mesoporous catalysts with moderate specific surface area, over 120 $m^2 \cdot g^{-1}$ in all cases, and uniformly dispersed metallic nanoparticles with particle sizes ranging from 4 to 6 nm, as evidenced by N_2 adsorption-desorption isotherms and HR-TEM images, respectively. The catalysts were tested in propane oxidative conversion in the absence and presence of CO_2, showing improved catalytic performances when Cr or Ga were added to the catalyst formulation despite their low metal loading. Without CO_2, all catalysts presented deactivation with time on stream, especially the most active catalyst, Cr-PCA. In terms of selectivity and therefore conversion routes, propylene was the main product followed by ethylene, indicating that propane conversion took place via direct dehydrogenation but also via propane cracking in the absence of CO_2. In the presence of CO_2, the stability of all catalysts was enhanced, with Cr-PCA also being the most active catalyst, although in terms of selectivity the opposite trend was found, with ethylene being the main product followed by propylene, indicating that in this case CO_2-assisted propane cracking is the main reaction route, followed by CO_2-ODH. The

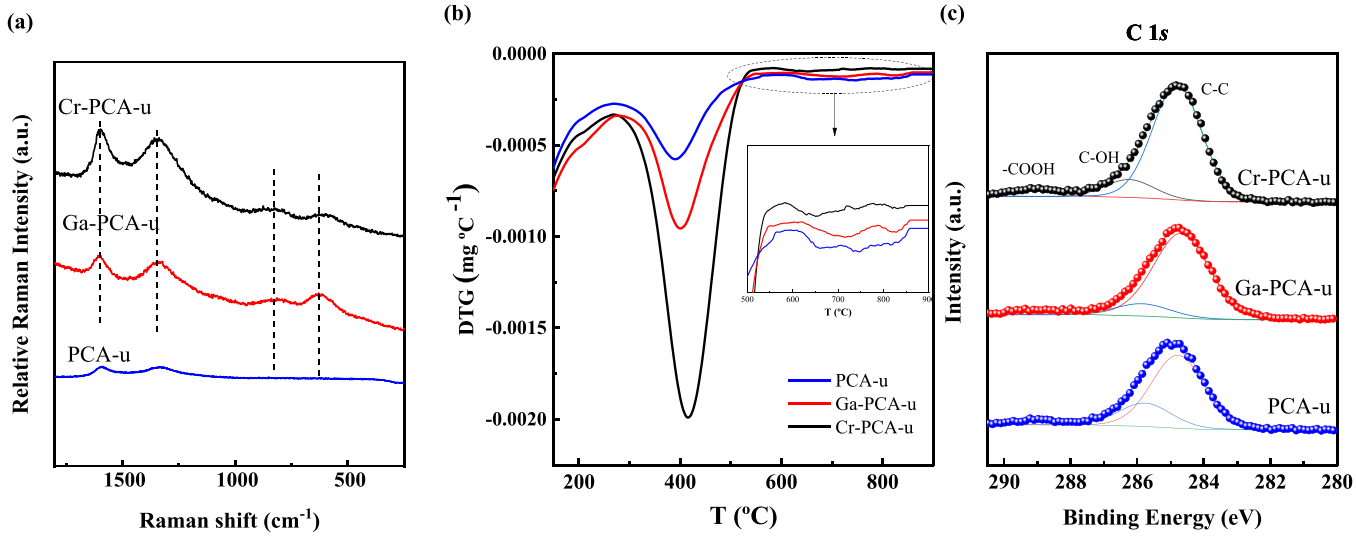

Fig. 8. (a) Raman spectra, (b) DTG profiles and (c) C 1 *s* core level spectra for prepared catalyst after reaction in the presence of CO_2.

better catalytic performance of the Cr-PCA catalyst was attributed to its weak nature acidity, uniformly dispersed active phases and the coexistence of Cr^{3+} and Cr^{6+} species, conferring redox properties and thus promoting oxygen mobility over this catalyst. The second most active catalyst was Ga-PCA, with higher selectivity to propylene, indicating that higher acidity of weak-to-medium nature together with the formation of Ga^{3+} species is beneficial for the CO_2-ODH process, also having into account the ratio CO/C_3H_6 closed to 1. Characterization results of the used catalysts showed that the catalysts' deactivation was due to the deposition of carbonaceous species of amorphous and graphitic nature according to Raman, DTG and XPS analysis, hindering propane's access to the active sites. In fact, CO_2 conversion data evidenced that CO_2 was also a byproduct generated by undesired side reactions like water gas shift and Boudouard reactions, which could worsen coke deposition and propylene selectivity.

CRediT authorship contribution statement

J.M. López Nieto: Writing – review & editing, Supervision, Investigation, Funding acquisition. **E. Rodríguez-Castellón:** Writing – review & editing, Investigation, Funding acquisition, Formal analysis. **A. Infantes-Molina:** Writing – review & editing, Supervision, Investigation, Funding acquisition, Formal analysis. **D. Ballesteros-Plata:** Writing – original draft, Formal analysis, Data curation, Conceptualization. **I. Barroso-Martín:** Writing – review & editing, Writing – original draft, Formal analysis, Data curation. **J.A. Cecilia:** Supervision, Methodology, Investigation, Conceptualization. **P. Concepción:** Writing – review & editing, Investigation, Funding acquisition.

Declaration of Competing Interest

The authors declare that they have no known competing financial interests or personal relationships that could have appeared to influence the work reported in this paper.

Acknowledgements

The authors thank the funding received from the Spanish Ministry of Science and Innovation, PID2021-126235OB-C31 and PID2021-126235OB-C32 funded by MCIN/ AEI/10.13039/501100011033 and FEDER funds, and projects TED2021–130756B-C31 and TED2021-130756B-C32 funded by MCIN/AEI/10.13039/501100011033 and by "ERDF A way of making Europe" by the European Union NextGenerationEU/PRTR. IBM thanks Universidad de Málaga for a postdoctoral grant.

Data Availability

Data will be made available on request.

References

[1] S. Wang, Z.H. Zhu, Catalytic conversion of alkanes to olefins by carbon dioxide oxidative dehydrogenation - a review, Energy Fuels 18 (2004) 1126–1139, https://doi.org/10.1021/ef0340716.
[2] S. Kawi, Y. Kathiraser, CO_2 as an oxidant for high-temperature reactions, Front. Energy Res. 3 (2015) 1–17, https://doi.org/10.3389/fenrg.2015.00013.
[3] V. Havran, M.P. Duduković, C.S. Lo, Conversion of methane and carbon dioxide to higher value products, Ind. Eng. Chem. Res. 50 (2011) 7089–7100, https://doi.org/10.1021/ie2000192.
[4] E. Gomez, Z. Xie, J.G. Chen, The effects of bimetallic interactions for CO_2-assisted oxidative dehydrogenation and dry reforming of propane, AIChE J. 65 (2019) 1–12, https://doi.org/10.1002/aic.16670.
[5] MRFR, Light Olefins Market Research Report –Global Forecast to 2030, (n.d.). ⟨https://www.marketresearchfuture.com/reports/light-olefin-market-1037⟩.
[6] H.H. Chiu, B.Y. Yu, Synthesis of green light olefins from direct hydrogenation of CO_2. Part I: Techno-economic, decarbonization, and sustainability analyses based on rigorous simulation, J. Taiwan Inst. Chem. Eng. 156 (2024) 105340, https://doi.org/10.1016/J.JTICE.2023.105340.
[7] Y. Ramesh, P. Thirumala Bai, B. Hari Babu, N. Lingaiah, K.S. Rama Rao, P.S. S. Prasad, Oxidative dehydrogenation of ethane to ethylene on Cr_2O_3/Al_2O_3–ZrO_2 catalysts: the influence of oxidizing agent on ethylene selectivity, Appl. Petrochem. Res. 4 (2014) 247–252, https://doi.org/10.1007/s13203-014-0043-4.
[8] C.A. Carrero, R. Schloegl, I.E. Wachs, R. Schomaecker, Critical literature review of the kinetics for the oxidative dehydrogenation of propane over well-defined supported vanadium oxide catalysts, ACS Catal. 4 (2014) 3357–3380, https://doi.org/10.1021/cs5003417.
[9] F. Cavani, N. Ballarini, A. Cericola, Oxidative dehydrogenation of ethane and propane: How far from commercial implementation? Catal. Today 127 (2007) 113–131, https://doi.org/10.1016/j.cattod.2007.05.009.
[10] M.A. Atanga, F. Rezaei, A. Jawad, M. Fitch, A.A. Rownaghi, Oxidative dehydrogenation of propane to propylene with carbon dioxide, Appl. Catal. B Environ. 220 (2018) 429–445, https://doi.org/10.1016/j.apcatb.2017.08.052.
[11] M. Chen, J.L. Wu, Y.M. Liu, Y. Cao, L. Guo, H.Y. He, K.N. Fan, Study in support effect of In_2O_3/MO_x (M = Al, Si, Zr) catalysts for dehydrogenation of propane in the presence of CO_2, Appl. Catal. A Gen. 407 (2011) 20–28, https://doi.org/10.1016/j.apcata.2011.08.018.
[12] R. Grabowski, Kinetics of oxidative dehydrogenation of C2-C3 alkanes on oxide catalysts, Catal. Rev. - Sci. Eng. 48 (2006) 199–268, https://doi.org/10.1080/01614940600631413.
[13] J. Santamaría-González, J. Mérida-Robles, M. Alcántara-Rodríguez, P. Maireles-Torres, E. Rodríguez-Castellón, A. Jiménez-López, Catalytic behaviour of chromium supported mesoporous MCM-41 silica in the oxidative dehydrogenation of propane, Catal. Lett. 64 (2000) 209–214, https://doi.org/10.1023/A:1019019927560.
[14] F. Cavani, F. Trifirò, The oxidative dehydrogenation of ethane and propane as an alternative way for the production of light olefins, Catal. Today 24 (1995) 307–313, https://doi.org/10.1016/0920-5861(95)00051-G.
[15] Ž.S. Kotanjac, M. van Sint Annaland, J.A.M. Kuipers, A packed bed membrane reactor for the oxidative dehydrogenation of propane on a Ga_2O_3/MoO_3 based catalyst, Chem. Eng. Sci. 65 (2010) 441–445, https://doi.org/10.1016/j.ces.2009.04.015.
[16] T. Davies, S.H. Taylor, The oxidative dehydrogenation of propane using gallium-molybdenum oxide-based catalysts, J. Mol. Catal. A Chem. 220 (2004) 77–84, https://doi.org/10.1016/j.molcata.2004.01.027.
[17] I. Ascoop, V.V. Galvita, K. Alexopoulos, M.F. Reyniers, P. Van Der Voort, V. Bliznuk, G.B. Marin, The role of CO_2 in the dehydrogenation of propane over WO_x-VO_x/SiO_2, J. Catal. 335 (2016) 1–10, https://doi.org/10.1016/j.jcat.2015.12.015.
[18] D. Mukherjee, S.E. Park, B.M. Reddy, CO_2 as a soft oxidant for oxidative dehydrogenation reaction: an eco benign process for industry, J. CO_2 Util. 16 (2016) 301–312, https://doi.org/10.1016/j.jcou.2016.08.005.
[19] ⟨https://www.epa.gov/ghgemissions/overview-greenhouse-gases#CO2-references⟩, Visit. 22-09-2022. (n.d.).
[20] J. Kang, A.D. Czaja, V.V. Guliants, Carbon dioxide as feedstock in selective oxidation of propane, Eur. J. Inorg. Chem. 2017 (2017) 4757–4762, https://doi.org/10.1002/ejic.201701049.
[21] J.N. Armor, Emerging importance of shale gas to both the energy & chemicals landscape, J. Energy Chem. 22 (2013) 21–26, https://doi.org/10.1016/S2095-4956(13)60002-9.
[22] A.M. Ranjekar, G.D. Yadav, Dry reforming of methane for syngas production: a review and assessment of catalyst development and efficacy, J. Indian Chem. Soc. 98 (2021) 100002, https://doi.org/10.1016/j.jics.2021.100002.
[23] Fibers Polyesters, Encycl. Polym. Sci. Technol. 3 (2002) 678–703.
[24] G. Li, C. Liu, X. Cui, Y. Yang, F. Shi, Oxidative dehydrogenation of light alkanes with carbon dioxide, Green. Chem. 23 (2021) 689–707, https://doi.org/10.1039/d0gc03705b.
[25] J.H. Carter, T. Bere, J.R. Pitchers, D.G. Hewes, B.D. Vandegehuchte, C.J. Kiely, S. H. Taylor, G.J. Hutchings, Direct and oxidative dehydrogenation of propane: From catalyst design to industrial application, Green. Chem. 23 (2021) 9747–9799, https://doi.org/10.1039/d1gc03700e.
[26] O.V. Krylov, A.K. Mamedov, S.R. Mirzabekova, Catalytic oxidation of hydrocarbons and alcohols by carbon dioxide on oxide catalysts, Ind. Eng. Chem. Res. 34 (1995) 474–482, https://doi.org/10.1021/ie00041a007.
[27] S. Sato, M. Ohhara, T. Sodesawa, F. Nozaki, Combination of ethylbenzene dehydrogenation and carbon dioxide shift-reaction over a sodium oxide/alumina catalyst, Appl. Catal. 37 (1988) 207–215, https://doi.org/10.1016/S0166-9834(00)80761-7.
[28] D. Pakhare, J. Spivey, A review of dry (CO_2) reforming of methane over noble metal catalysts, Chem. Soc. Rev. 43 (2014) 7813–7837, https://doi.org/10.1039/c3cs60395d.
[29] X. Jiang, L. Sharma, V. Fung, S.J. Park, C.W. Jones, B.G. Sumpter, J. Baltrusaitis, Z. Wu, Oxidative dehydrogenation of propane to propylene with soft oxidants via heterogeneous catalysis, ACS Catal. 11 (2021) 2182–2234, https://doi.org/10.1021/acscatal.0c03999.
[30] Y. Gambo, S. Adamu, G. Tanimu, I.M. Abdullahi, R.A. Lucky, M.S. Ba-Shammakh, M.M. Hossain, CO_2-mediated oxidative dehydrogenation of light alkanes to olefins: Advances and perspectives in catalyst design and process improvement, Appl. Catal. A: Gen. 623 (2021) 118273, https://doi.org/10.1016/j.apcata.2021.118273.
[31] F. Feng, H. Zhang, S. Chu, Q. Zhang, C. Wang, G. Wang, F. Wang, L. Bing, D. Han, Recent progress on the traditional and emerging catalysts for propane dehydrogenation, J. Ind. Eng. Chem. 118 (2023) 1–18, https://doi.org/10.1016/J.JIEC.2022.11.001.

[32] E. Gomez, B. Yan, S. Kattel, J.G. Chen, Carbon dioxide reduction in tandem with light-alkane dehydrogenation, Nat. Rev. Chem. 3 (2019) 638–649, https://doi.org/10.1038/s41570-019-0128-9.

[33] T. Otroshchenko, G. Jiang, V.A. Kondratenko, U. Rodemerck, E.V. Kondratenko, Current status and perspectives in oxidative, non-oxidative and CO_2-mediated dehydrogenation of propane and isobutane over metal oxide catalysts, Chem. Soc. Rev. 50 (2021) 473–527, https://doi.org/10.1039/d0cs01140a.

[34] H. Saito, Y. Sekine, Catalytic conversion of ethane to valuable products through non-oxidative dehydrogenation and dehydroaromatization, RSC Adv. 10 (2020) 21427–21453, https://doi.org/10.1039/d0ra03365k.

[35] R. Watanabe, Y. Hondo, K. Mukawa, C. Fukuhara, E. Kikuchi, Y. Sekine, Stable and selective perovskite catalyst for dehydrogenation of propane working with redox mechanism, J. Mol. Catal. A Chem. 377 (2013) 74–84, https://doi.org/10.1016/J.MOLCATA.2013.04.033.

[36] Y.A. Agafonov, N.A. Gaidai, A.L. Lapidus, Influence of the preparation conditions for catalysts CrO_x/SiO_2 on their efficiency in propane dehydrogenation in the presence CO_2, Russ. Chem. Bull. 63 (2014) 381–388, https://doi.org/10.1007/s11172-014-0441-x.

[37] Z. Zhai, X. Wang, R. Licht, A.T. Bell, Selective oxidation and oxidative dehydrogenation of hydrocarbons on bismuth vanadium molybdenum oxide, J. Catal. 325 (2015) 87–100, https://doi.org/10.1016/j.jcat.2015.02.015.

[38] A. Talati, M. Haghighi, F. Rahmani, Impregnation: Vs. coprecipitation dispersion of Cr over TiO_2 and ZrO_2 used as active and stable nanocatalysts in oxidative dehydrogenation of ethane to ethylene by carbon dioxide, RSC Adv. 6 (2016) 44195–44204, https://doi.org/10.1039/c6ra05049b.

[39] J. Baek, H.J. Yun, D. Yun, Y. Choi, J. Yi, Preparation of highly dispersed chromium oxide catalysts supported on mesoporous silica for the oxidative dehydrogenation of propane using CO 2: Insight into the nature of catalytically active chromium sites, ACS Catal. 2 (2012) 1893–1903, https://doi.org/10.1021/cs300198u.

[40] E. Gomez, S. Kattel, B. Yan, S. Yao, P. Liu, J.G. Chen, Combining CO_2 reduction with propane oxidative dehydrogenation over bimetallic catalysts, Nat. Commun. 9 (2018) 1–6, https://doi.org/10.1038/s41467-018-03793-w.

[41] R. Wu, N. Liu, C. Dai, G. Yu, R. Xu, B. Chen, CO in situ directed highly efficient CrOx@silicalite-1 for propane oxidation dehydrogenation by CO_2, Catal. Today 436 (2024) 114746, https://doi.org/10.1016/J.CATTOD.2024.114746.

[42] R.A. Meyers, UOP CYCLAR PROCESS, McGraw-Hill Education, 2016. ⟨https://www.accessengineeringlibrary.com/content/book/9780071850490/chapter/chapter8⟩ (accessed July 29, 2024).

[43] A. Sanna, T.P. Vispute, G.W. Huber, Hydrodeoxygenation of the aqueous fraction of bio-oil with Ru/C and Pt/C catalysts, Appl. Catal. B Environ. 165 (2015) 446–456, https://doi.org/10.1016/j.apcatb.2014.10.013.

[44] P. Michorczyk, J. Ogonowski, Dehydrogenation of propane to propene over gallium oxide in the presence of CO_2, Appl. Catal. A Gen. 251 (2003) 425–433, https://doi.org/10.1016/S0926-860X(03)00368-5.

[45] P. Castro-Fernández, D. Mance, C. Liu, I.B. Moroz, P.M. Abdala, E.A. Pidko, C. Copéret, A. Fedorov, C.R. Müller, Propane Dehydrogenation on Ga_2O_3-Based Catalysts: Contrasting Performance with Coordination Environment and Acidity of Surface Sites, ACS Catal. 11 (2021) 907–924, https://doi.org/10.1021/ACSCATAL.0C05009/ASSET/IMAGES/LARGE/CS0C05009_0008.JPEG.

[46] A.S. Oliveira, J. Cueto, M. del M. Alonso-Doncel, M. Kubů, J. Čejka, D.P. Serrano, R. A. García-Muñoz, Propane dehydrogenation over Pt and Ga-containing MFI zeolites with modified acidity and textural properties, Catal. Today 427 (2024) 114437, https://doi.org/10.1016/J.CATTOD.2023.114437.

[47] C.H. Bartholomew, R.J. Farrauto, Catalytic Processes, 2nd Edition, 85 (2007) 2006–2007.

[48] R.X. Valenzuela, G. Bueno, V. Cortés Corberán, Y. Xu, C. Chen, Selective oxidehydrogenation of ethane with CO_2 over CeO_2-based catalysts, Catal. Today 61 (2000) 43–48, https://doi.org/10.1016/S0920-5861(00)00366-7.

[49] E. Nowicka, C. Reece, S.M. Althahban, K.M.H. Mohammed, S.A. Kondrat, D. J. Morgan, Q. He, D.J. Willock, S. Golunski, C.J. Kiely, G.J. Hutchings, Elucidating the role of CO_2 in the soft oxidative dehydrogenation of propane over ceria-based catalysts, ACS Catal. 8 (2018) 3454–3468, https://doi.org/10.1021/acscatal.7b03805.

[50] P. Al, M.S. Brogan, T.J. Dines, J.A. Cairns, Raman spectroscopic study of the Pt–CeO2 interaction in the Pt/Al_2O_3–CeO_2 catalyst, J. Chem. Soc. Faraday Trans. 90 (1994) 1461–1466, https://doi.org/10.1039/FT9949001461.

[51] M. o Sugino, H. Shimada, T. Turuda, H. Miura, N. Ikenaga, T. Suzuki, Oxidative dehydrogenation of ethylbenzene with carbon dioxide, Appl. Catal. A, Gen. 121 (1995) 125–137, https://doi.org/10.1016/0926-860X(95)85015-5.

[52] T. Badstube, H. Papp, P. Kustrowski, R. Dziembaj, Oxidative dehydrogenation of ethylbenzene with carbon dioxide on alkali-promoted Fe/active carbon catalysts, Catal. Lett. 55 (1998) 169–172, https://doi.org/10.1023/A:1019099332393.

[53] K. Nakagawa, C. Kajita, K. Okumura, N. oki Ikenaga, T. Suzuki, K. Nakagawa, T. Ando, T. Suzuki, M. Nishitani-Gamo, T. Ando, T. Kobayashi, Role of carbon dioxide in the dehydrogenation of ethane over gallium-loaded catalysts, J. Catal. 203 (2001) 87–93, https://doi.org/10.1006/JCAT.2001.3306.

[54] K.S.W. Sing, D.H. Everett, R.A.W. Haul, L. Moscou, R.A. Pierotti, T. Siemieniewska, Reporting physisorption data for gas/solid systems with special reference to the determination of surface area and porosity, Int. Union, Pure Appl. Chem. Phys. Chem. Div. Comm. Colloid Surf. Chem. Incl. Catal. 57 (1985) 603–619, https://doi.org/10.1351/pac198557040603.

[55] M.H. Jeong, J. So, J. Oh, K.M. Kim, J.H. Park, Y.W. You, J.H. Lee, I. Heo, Y.J. Kim, Cerium-modified Pt/Al_2O_3 for NH_3 synthesis by NO reduction with H_2, Appl. Surf. Sci. 638 (2023) 158067, https://doi.org/10.1016/J.APSUSC.2023.158067.

[56] M. Li, W. Li, Y. Yang, D. Yu, J. Lin, R. Wan, H. Zhu, Remarkably efficient Pt/CeO_2–Al_2O_3 catalyst for catalytic hydrodeiodination of monoiodoacetic acid: Synergistic effect of Al_2O_3 and CeO_2, Chemosphere 327 (2023) 138515, https://doi.org/10.1016/J.CHEMOSPHERE.2023.138515.

[57] Q.Y. Chen, N. Li, M.F. Luo, J.Q. Lu, Catalytic oxidation of dichloromethane over Pt/CeO_2–Al_2O_3 catalysts, Appl. Catal. B: Environ. 127 (2012) 159–166, https://doi.org/10.1016/J.APCATB.2012.08.020.

[58] S. Xie, X. Zhang, P. Xu, B. Hatcher, Y. Liu, L. Ma, S.N. Ehrlich, S. Hong, F. Liu, Effect of surface acidity modulation on Pt/Al_2O_3 single atom catalyst for carbon monoxide oxidation and methanol decomposition, Catal. Today 402 (2022) 149–160, https://doi.org/10.1016/J.CATTOD.2022.03.028.

[59] C. Lin, Z. Yang, H. Pan, J. Cui, Z. Lv, X. liu, P. Tian, Z. Xiao, P. Li, J. Xu, Y.F. Han, Ce-introduced effects on modification of acidity and Pt electronic states on Pt-Sn/γ-Al_2O_3 catalysts for catalytic reforming, Appl. Catal. A Gen. 617 (2021) 118116, https://doi.org/10.1016/J.APCATA.2021.118116.

[60] D.S. Wang, S.L. Zhang, L. Wei, Y.H. Lu, X.M. Jing, Preparation and characterization of hydrolysis component γ-Ga_2O_3 for hydrogen production by low temperature steam reforming of dimethyl ether in slurry reactor, J. Fuel Chem. Technol. 46 (2018) 666–672, https://doi.org/10.1016/S1872-5813(18)30029-X.

[61] S.P. Batchu, H.L. Wang, W. Chen, W. Zheng, S. Caratzoulas, R.F. Lobo, D. G. Vlachos, Ethane Dehydrogenation on Single and Dual Centers of Ga-modified γ-Al_2O_3, ACS Catal. 11 (2021) 1380–1391, https://doi.org/10.1021/ACSCATAL.0C03536/SUPPL_FILE/CS0C03536_SI_003.ZIP.

[62] X. Cai, Z. Zhang, L. Cai, X. Tian, W. Chu, W. Yang, Effect of Calcination Atmosphere on the Structure and Catalytic Behavior of Cr_2O_3/Al_2O_3 Catalysts for Dehydrogenation of Propane, Ind. Eng. Chem. Res. 61 (2022) 16479–16488, https://doi.org/10.1021/ACS.IECR.2C03031/ASSET/IMAGES/LARGE/IE2C03031_0010.JPEG.

[63] Y. Zhao, D. Chen, J. Liu, D. He, X. Cao, C. Han, J. Lu, Y. Luo, Tuning the metal-support interaction on chromium-based catalysts for catalytically eliminate methyl mercaptan: Anchored active chromium species through surface hydroxyl groups, Chem. Eng. J. 389 (2020) 124384, https://doi.org/10.1016/J.CEJ.2020.124384.

[64] Y. He, E. Guo, F. Zhong, B. Fu, G. Cai, D. Zhang, C. Jiang, F. Ren, A novel method for preparing α-Al_2O_3 (Cr_2O_3)/Fe–Al composite coating with high hydrogen isotopes permeation resistance, Ceram. Int. 50 (2024) 20367–20375, https://doi.org/10.1016/J.CERAMINT.2024.03.160.

[65] L.A. do Nascimento, Isabel Barroso-Martín, S.R.S. Peçanha, S. Arias, B.S. Santos, J. G.A. Pacheco, A. Infantes-Molina, E. Rodríguez-Castellón, I. de C.L. Barros, NiAlCe mixed oxides obtained from layered double hydroxides applied to anisole hydrodeoxygenation, Catal. Today 394–396 (2022) 282–294, https://doi.org/10.1016/J.CATTOD.2021.08.026.

[66] M.J. Kang, D.H. Yoon, Effects of surface hydroxyl ions on the color of sintered Al_2O_3 characterized by X-ray photoelectron and infrared spectroscopy, J. Eur. Ceram. Soc. 42 (2022) 7508–7515, https://doi.org/10.1016/J.JEURCERAMSOC.2022.09.016.

[67] S. Damyanova, J.M.C. Bueno, Effect of CeO_2 loading on the surface and catalytic behaviors of CeO_2-Al_2O_3-supported Pt catalysts, Appl. Catal. A Gen. 253 (2003) 135–150, https://doi.org/10.1016/S0926-860X(03)00500-3.

[68] E. Bêche, P. Charvin, D. Perarnau, S. Abanades, G. Flamant, Ce 3d XPS investigation of cerium oxides and mixed cerium oxide (Ce xTiyOz), Surf. Interface Anal. 40 (2008) 264–267, https://doi.org/10.1002/SIA.2686.

[69] R.A. Vazirov, S.Y. Sokovnin, V.G. Ilves, I.N. Bazhukova, N. Pizurova, M. V. Kuznetsov, Physicochemical characterization and antioxidant properties of cerium oxide nanoparticles, J. Phys. Conf. Ser. 1115 (2018) 0–6, https://doi.org/10.1088/1742-6596/1115/3/032094.

[70] Y. Tang, Y. Chen, A. Abid, Z. Meng, X. Sun, B. Li, Z. Zhao, Revisiting the origin of the superior performance of defective zirconium oxide catalysts in propane dehydrogenation: Double-edged oxygen vacancy, Chin. J. Catal. 68 (2025) 272–281, https://doi.org/10.1016/S1872-2067(24)60163-4.

[71] Y. Yue, X. Liu, M. Shakouri, Y. Hu, Y. Guo, Y. Wang, Active and stable Pt-Ga_2O_3/Al_2O_3 catalyst for dehydrogenation of methylcyclohexane, Catal. Today 433 (2024) 114688, https://doi.org/10.1016/J.CATTOD.2024.114688.

[72] M. Messaykeh, S. Chenot, P. David, G. Cabailh, J. Jupille, A. Koltsov, P. Lagarde, N. Trcera, J. Goniakowski, R. Lazzari, Core level shifts as indicators of Cr chemistry on hydroxylated α-Al2O3(0001): A combined photoemission and first-principles study, Phys. Chem. Chem. Phys. 23 (2021) 21852–21862, https://doi.org/10.1039/d1cp03224k.

[73] T. Greunz, H. Duchaczek, R. Sagl, J. Duchoslav, R. Steinberger, B. Strauß, D. Stifter, Quantification of the toxic hexavalent chromium content in an organic matrix by X-ray photoelectron spectroscopy (XPS) and ultra-low-angle microtomy (ULAM), Appl. Surf. Sci. 396 (2017) 665–671, https://doi.org/10.1016/j.apsusc.2016.11.004.

[74] G.P. Halada, C.R. Clayton, Photoreduction of Hexavalent Chromium during X-Ray Photoelectron Spectroscopy Analysis of Electrochemical and Thermal Films, J. Electrochem. Soc. 138 (1991) 2921–2927, https://doi.org/10.1149/1.2085340.

[75] Y. Zhang, M. Aly, Effect of CO_2 on activity and coke formation over gallium-based catalysts for propane dehydrogenation, Appl. Catal. A Gen. 643 (2022) 118795, https://doi.org/10.1016/J.APCATA.2022.118795.

[76] G. do, N. Franceschini, P. Concepción, M. Schwaab, M. do Carmo Rangel, J. Martínez-Triguero, J.M. López Nieto, Spectroscopic insights into the role of CO_2 on the nature of Cr species in a CrO_X/Al_2O_3 catalysts during ethane dehydrogenation with CO_2, Appl. Catal. A Gen. 661 (2023) 119260, https://doi.org/10.1016/J.APCATA.2023.119260.

[77] T. Shishido, K. Shimamura, K. Teramura, T. Tanaka, Role of CO 2 in dehydrogenation of propane over Cr-based catalysts, Catal. Today 185 (2012) 151–156, https://doi.org/10.1016/j.cattod.2011.10.028.

[78] C.C. Zhang, S. Hartlaub, I. Petrovic, B. Yilmaz, Raman Spectroscopy Characterization of Amorphous Coke Generated in Industrial Processes, ACS Omega 7 (2022) 2565–2570, https://doi.org/10.1021/acsomega.1c03456.
[79] J. Mcgregor, Z. Huang, E.P.J. Parrott, J.A. Zeitler, K.L. Nguyen, J.M. Rawson, A. Carley, T.W. Hansen, J. Tessonnier, D. Sheng, D. Teschner, E.M. Vass, A. Knopgericke, R. Schlögl, L.F. Gladden, Active coke: Carbonaceous materials as catalysts for alkane dehydrogenation, J. Catal. 269 (2010) 329–339, https://doi.org/10.1016/j.jcat.2009.11.016.
[80] A.C. Ferrari, J. Robertson, Interpretation of Raman spectra of disordered and amorphous carbon, Phys. Rev. B. 61 (2000) 95–107, https://doi.org/10.1103/physrevb.61.14095.
[81] J.A. Cecilia, E. Vilarrasa-García, D.C.S. Azevedo, A. Vílchez-Cózar, A. Infantes-Molina, D. Ballesteros-Plata, I. Barroso-Martín, E. Rodríguez-Castellón, Valorization of wipe wastes for the synthesis of microporous carbons and their application in CO_2 capture, gas separation and H2-storage, 1–13, Heliyon 9 (2023), https://doi.org/10.1016/j.heliyon.2023.e20606.
[82] H. Vaskova, Raman Microsc. Detect. Chromium Compd. 05012 (2016) 4–7.
[83] W. Tan, S. Xie, X. Wang, C. Wang, Y. Li, T.E. Shaw, L. Ma, S.N. Ehrlich, A. Liu, J. Ji, F. Gao, L. Dong, F. Liu, Highly efficient Pt catalyst on newly designed CeO_2-ZrO_2-Al_2O_3 support for catalytic removal of pollutants from vehicle exhaust, Chem. Eng. J. 426 (2021) 131855, https://doi.org/10.1016/J.CEJ.2021.131855.
[84] J. Guo, Z. Shi, D. Wu, H. Yin, M. Gong, Y. Chen, Study of Pt–Rh/ CeO_2-ZrO_2–M_xO_y (M = Y, La)/Al2O3 three-way catalysts, Appl. Surf. Sci. 273 (2013) 527–535, https://doi.org/10.1016/J.APSUSC.2013.02.074.
[85] D. Ballesteros-Plata, A. Infantes-Molina, E. Rodríguez-Castellón, M.A. Cauqui, M. P. Yeste, Improving noble metal catalytic activity in the dry reforming of methane by adding niobium, Fuel 308 (2022) 121996, https://doi.org/10.1016/J.FUEL.2021.121996.
[86] X. Huang, W. Mo, X. He, X. Fan, F. Ma, D. Tax, Effects of promoters on the structure, performance, and carbon deposition of Ni-Al_2O_3 catalysts for CO_2-CH_4 reforming, ACS Omega 6 (2021) 16381–16390, https://doi.org/10.1021/ACSOMEGA.1C00918/ASSET/IMAGES/LARGE/AO1C00918_0014.JPEG.
[87] Z. Lin, H. Zuo, R. Ma, H. An, P. Zhao, K. Liang, M. Wang, F. Lu, G. Zou, The evolution of surface species by steam pre-treatment on CrO_x/Al_2O_3 catalysts for propane dehydrogenation, Mol. Catal. 539 (2023) 113018, https://doi.org/10.1016/J.MCAT.2023.113018.
[88] B. Pawelec, S. Damyanova, K. Arishtirova, J.L.G. Fierro, L. Petrov, Structural and surface features of PtNi catalysts for reforming of methane with CO_2, Appl. Catal. A Gen. 323 (2007) 188–201, https://doi.org/10.1016/J.APCATA.2007.02.017.